JOURNAL OF VIROLOGY, July 2004, p. 7186–7198 Vol. 78, No. 13
0022-538X/04/$08.00+0 DOI: 10.1128/JVI.78.13.7186–7198.2004

Receptor (CD155)-Dependent Endocytosis of Poliovirus and Retrograde Axonal Transport of the Endosome

Seii Ohka,[1] Norie Matsuda,[1] Koujiro Tohyama,[2] Toshiyuki Oda,[1] Masato Morikawa,[1] Shusuke Kuge,[1] and Akio Nomoto[1]*

Department of Microbiology, Graduate School of Medicine, The University of Tokyo, Bunkyo-ku, Tokyo 113-0033,[1] and The Center for Electron Microscopy and Bio-Imaging Research, Department of Neuroanatomy, Iwate Medical University, Morioka, Iwate 020-8505,[2] Japan

Received 19 November 2003/Accepted 18 February 2004

Poliovirus (PV), when injected intramuscularly into the calf, is incorporated into the sciatic nerve and causes an initial paralysis of the inoculated limb in transgenic mice carrying the human PV receptor (hPVR/CD155) gene. Here, we demonstrated by using an immunoelectron microscope that PV particles exist on vesicle structures in nerve terminals of neuromuscular junctions. We also demonstrated in glutathione *S*-transferase pull-down experiments that the dynein light chain, Tctex-1, interacts directly with the cytoplasmic domain of hPVR. In the axons of differentiated rat PC12 cells transfected with expression vectors for hPVRs, vesicles composed of PV and hPVRα, as well as a mutant hPVRα (hPVRMα) that had a reduced ability to bind Tctex-1, colocalized with Tctex-1. However, vesicles containing PV, dextran, and hPVRα had only retrograde motion, while those containing PV, dextran, and hPVRMα had anterograde or retrograde motion. Topical application of the antimicrotubule agent vinblastine to the sciatic nerve reduced the amount of virus transported from the calf to the spinal cord. These results suggest that direct efficient interaction between the cytoplasmic domain and Tctex-1 is essential for the efficient retrograde transport of PV-containing vesicles along microtubules in vivo.

In humans, paralytic poliomyelitis is considered to result from an invasion by circulating poliovirus (PV) into the central nervous system, probably via the blood-brain barrier. The notion is supported by a previous study using a mouse model (44). In that study, it was demonstrated that circulating PV after intravenous inoculation appears to cross the blood-brain barrier at a high rate, and the neural dissemination pathway from the skeletal muscle is not the primary dissemination route of the circulating virus to the central nervous system. Along with this pathway of dissemination, a neural pathway has been reported in humans (32), monkeys (20), and PV-sensitive transgenic (Tg) mice carrying the human PV receptor (hPVR/CD155) gene (35, 36), and it appears to be important in causing provocation poliomyelitis (14). Using the Tg mouse line, we demonstrate that PV inoculated into the calf is incorporated into the sciatic nerve and retrogradely transported through the axons as intact virion particles, that one of the fast retrograde axonal transport systems is involved in viral dissemination, and that the pathogenesis of PV infection via the neural pathway is inhibited by the anti-hPVR monoclonal antibody (MAb) p286, which is able to block the infection (35).

hPVR is a member of the immunoglobulin (Ig) superfamily, with three linked extracellular Ig-like domains followed by a membrane-spanning domain and a cytoplasmic domain (CP). Two membrane-bound forms (hPVRα and hPVRδ) and two secreted forms (hPVRβ and hPVRγ) derived by alternative splicing are potentially expressed in human cells (28). Membrane-bound hPVRs are considered to play important roles in the early steps of infection, such as binding of the virus to the cell surface, penetration of the cell, and uncoating of the virus. The N-terminal extracellular Ig-like domain harbors the sites for the binding of PV and anti-hPVR MAbs that block PV infection (12, 29, 37).

It has been suggested that the CP of hPVR has several functions in polarized cells. We have reported that the tyrosine motif exists only in the amino acid sequence specific to the CP of hPVRα (CPα) and that the motif is responsible for basolateral sorting of hPVRα in polarized epithelial cells (34). It has also been shown that the hPVR CP associates with TCTEL1 (31, 33), the human homolog of mouse Tctex-1 (41), and it is likely that they interact directly (31). In this report, Tctex-1 refers to the human protein TCTEL1. Tctex-1 has proven to be a light chain of the cytoplasmic dynein motor complex (27). Cytoplasmic dynein, a minus-end-directed microtubule-based motor protein (16–18, 40), interacts with a variety of structures, such as late endosomes, lysosomes, the Golgi complex, synaptic vesicles, and the endoplasmic reticulum, and is implicated in the transport of these organelles and vesicle transport between the organelles along microtubules (1, 16–18, 40). A hypothesis for the neural pathway of PV has been proposed as follows (31, 33). Intramuscularly (i.m.)-inoculated PV is incorporated into neural cells by hPVR-mediated endocytosis at synapses. The hPVR CP on the surfaces of endosomes that enclose intact PV interacts with cytoplasmic dynein, and the endosomes are retrogradely transported along microtubules through the axon to the neural-cell body, where the uncoating and replication of PV occur.

Here, we employ differentiated PC12 cells and a PV-sensitive Tg mouse line to gain insights into the mechanisms for hPVR-dependent incorporation of PV at synapses and the

* Corresponding author. Mailing address: Department of Microbiology, Graduate School of Medicine, The University of Tokyo, 7-3-1 Hongo, Bunkyo-ku, Tokyo 113-0033, Japan. Phone: 81-3-5841-3407. Fax: 81-3-5841-3374. E-mail: anomoto@m.u-tokyo.ac.jp.

axonal transport of the virus. Our results demonstrate that i.m.-inoculated PV is incorporated into neural cells by endocytosis at synapses and strongly suggest that efficient direct interaction of hPVR CP with Tctex-1 plays an important role in retrograde transport and that microtubules are involved in the transport of PV-containing vesicles. Thus, the data presented here strongly support the hypothesis described above (31, 33).

MATERIALS AND METHODS

Viruses and cells. A virulent Mahoney strain of type 1 PV derived from an infectious cDNA clone, pOM1, was used (38). African green monkey kidney cells were grown in Dulbecco modified Eagle medium (DMEM) supplemented with 5% newborn calf serum and used for the preparation of viruses, transfection experiments with infectious cDNA clones, and plaque assays. PC12 cells are a commonly used neuronal tissue culture cell line originally derived from a rat pheochromocytoma (13). Stock cells were grown in collagen-coated bottles in DMEM supplemented with 10% horse serum and 10% fetal calf serum at 37°C in 5% CO_2. When grown in a standard tissue culture medium, PC12 cells have a chromaffin-like appearance; however, after transfer into serum-free medium containing nerve growth factor (NGF), the cells extend neurites that are similar to axons. The PC12 cell line used here (subclone PC12D [24]) is particularly responsive to induction by NGF.

PC12 cells were transiently transfected following a standard cationic lipid-based DNA delivery protocol. In brief, 6 μl of DOTAP transfection reagent (Roche Diagnostics) was combined with 14 μl of HEPES-buffered saline 1 (HBS 1) (20 mM HEPES [cell culture grade], 150 mM NaCl [pH 7.4]), and 2 μg of DNA was diluted in 10 μl of HBS 1. The two solutions were combined, mixed gently, and allowed to stand for 15 min at room temperature (RT). The DOTAP-DNA complex was then added to 50 μl of newly displaced DMEM on 10^5 cells grown on collagen-coated 96-well plates. After incubation at 37°C for 14 h, the medium was replaced with fresh DMEM; 6 h later, cells in serum-free N_2 medium (Invitrogen Co.) (5) were split onto 10-mm-diameter glass bottom culture dishes (Mat Tek Co.) that had been coated with a thin layer of Matrigel (Becton Dickinson Labware) at 1 mg/ml. Twenty-four hours after their transfer to N_2, the cells were induced to differentiate with 50 ng of NGF (Invitrogen Co.)/ml. The differentiated cells were subjected to further experiments 2 days after the addition of NGF.

Construction of DNAs. The plasmid pPVRα-GFP, which encodes hPVRα-green fluorescent protein (GFP), was constructed from pEGFP-N1 (Clontech). Using a sense primer (nucleotides [nt] 556 to 575 of hPVRα cDNA; 5′-ATG CCC AAT ACG AGC CAG GT-3′) and an antisense primer containing a SalI restriction site (5′-TAC CGT CGA CCC CCT TGT GCC CTC TGT CTG T-3′), PCR was performed with pSV2PVRα (28) as a template. A KpnI (nt 764 of hPVRα cDNA)-SalI (C terminus of hPVRα cDNA) fragment encoding the C-terminal portion of hPVRα without a termination codon derived from the PCR product and a HindIII (N terminus of hPVRα cDNA)-KpnI (nt 764 of hPVRα cDNA) fragment encoding the N-terminal portion of hPVRα from pSV2PVRα were inserted into the HindIII-SalI site of pEGFP-N1 carrying the enhanced-GFP coding sequence.

The plasmid pPVRMα-GFP was constructed from pPVRα-GFP. Using a sense primer (nt 228 to 245 of hPVRα cDNA; 5′-CGT CTT CCA CCA AAC GCA-3′) and an antisense primer designed to substitute ACSA for KCSR (5′-TGT ACT CGA GGG ACA CAG ATG ACA GTG CCA AAG GAC CTC AGC GGA ACA AGC GGA CCA ATA GAA ATA AAT CCC G-3′), PCR was performed with pPVRα-GFP as a template. Independently, using a sense primer (nt 1134 to 1152 of hPVRα cDNA; 5′-TCA TCT GTG TCC CTC GAG T-3′) and an antisense primer for the C terminus of the hPVRα cDNA containing a SalI restriction site (5′-TAC CGT CGA CCC CCT TGT GCC CTC TGT CTG T-3′), PCR was performed with pPVRα-GFP as a template. The fragments derived from these reactions were mixed, and PCR was performed with a sense primer (nt 228 to 245 of hPVRα cDNA) and an antisense primer for the C terminus of hPVRα cDNA containing a SalI restriction site (5′-TAC CGT CGA CCC CCT TGT GCC CTC TGT CTG T-3′). An EcoRI (nt 277 of hPVRα cDNA)-SalI (C terminus of hPVRα cDNA) fragment derived from this PCR product was inserted into the EcoRI-SalI site of pPVRα-GFP. The sequence of the PCR fragment was confirmed using a DNA sequencer (PRISM 310; Applied Biosystems).

Tg mice. The Tg mouse line IQI-PVRTg21 (Tg21) (19, 30) in the hemizygous stage with IQI mice was used as an animal model for studying the neural pathway of PV infection. All mice used were free from specific pathogens and were 6 to 10 weeks of age. The mice were treated according to the Guidelines for the Care and Use of Laboratory Animals of The University of Tokyo.

Sciatic nerve treatment with vinblastine and inoculation of virus. After the Tg mice had been anesthetized with an intraperitoneal injection of 300 to 400 μl of ketamine (10 mg/ml) and xyladine (0.2 mg/ml) in saline, the left sciatic nerve along the thighbone was exposed. The sciatic nerve was surrounded with cotton soaked in 0.15 mM vinblastine (Sigma Chemical Co.) in PBS(−) (NaCl, 8.00 g; Na_2HPO_4, 1.15 g; KCl, 0.20 g; $MgCl_2 \cdot 6H_2O$, 0.10 g; KH_2PO_4, 0.20 g per liter [pH 7.4]) or PBS(−) alone for 15 min (23, 45). It has been shown that the sciatic nerve is not damaged by this treatment. After the cotton was removed, the region was rinsed three times with PBS(−). The next day, the Tg mice were i.m. inoculated with 5 μl of PV (10^6 PFU) in the left or right calf with a Hamilton microsyringe under anesthesia. The spinal cords of these mice were collected 16 h after the inoculation. The spinal cords were homogenized with a homogenization pestle (Scientific Specialties Inc.), followed by centrifugation, and the supernatant was used for the plaque assay.

Yeast two-hybrid analysis. Yeast cells were grown in YPAD (1% yeast extract, 2% peptone, 0.004% adenine sulfate, and 2% glucose) or in synthetic medium supplemented with amino acids (4). The yeast cells were transformed by the lithium acetate method essentially as described by Ito et al. (21).

The nucleotide sequence corresponding to the CP (1 to 50 amino acids [aa]) of PVRα cDNA was inserted into pGBT9 (pGBT9-PVRCP). The yeast reporter strain was HF7c with integrated growth selection (selection marker HIS3) and β-galactosidase (*lacZ*) reporter genes. For cDNA library screening, yeast cells were first transfected with pGBT9-PVRCP and subsequently transfected with a HeLa cDNA library constructed in pGADGH (Clontech). Colonies that grew in the absence of histidine were screened for β-galactosidase activity. cDNA plasmids were released from positive yeast colonies and cloned and sequenced with a Pharmacia AutoRead Sequencing kit according to the manufacturer's instructions. Transfectants were streaked on agarose medium lacking histidine to test for growth reporter activation or on medium containing histidine to test for activation of the *lacZ* reporter. The clones containing the putative full-length coding region of Tctex-1 were isolated by screening a HeLa cDNA library. A cDNA fragment encoding Tctex-1 was inserted into pGADGH. The cDNA fragments encoding mutants of CPα and hPVRδ CP (CPδ) were inserted into pGBT9. After cotransformation into yeast strain MaV203, growth reporter activity was measured as the growth on the agarose medium lacking histidine and quantified using β-galactosidase activity.

The β-galactosidase filter assay was performed as follows (3). Yeast strains were streaked on sheets of Hybond-N filter (Amersham Biosciences) on YPAD agar. After being incubated overnight at 30°C, the sheets were frozen in liquid N_2 and melted. They were then immersed in Z buffer (10 mM KCl, 60 mM Na_2HPO_4, 40 mM NaH_2PO_4, and 1 mM $MgSO_4$) with 1 mg of X-Gal (5-bromo-4-chloro-3-indolyl-β-D-galactopyranoside)/ml and again incubated overnight at 30°C. The reaction was stopped by adding 1 M Na_2CO_3.

Protein expression and purification. The glutathione *S*-transferase (GST) fusion proteins GST-His_6-CPα, GST-His_6, and GST-Tctex-1, and pFast Bac HTb GST CPα, pFast Bac HTb GST, and pFast Bac HTb GST Tctex-1 were constructed using pSV2PVRα and standard cloning techniques as follows. pGEX-6P-2 (Amersham Biosciences) was used as a template for the amplification of coding sequences for GST with primers designed to introduce flanking RsrII sites. The resulting PCR product was digested with RsrII and ligated into the appropriately digested pFast Bac HTb vector (Gibco-Invitrogen Co.) to yield pFast Bac HTb GST. pSV2-hPVRα was used as a template to amplify coding sequences for CPα with primers designed to introduce flanking EcoRI and SalI sites. The resulting product was inserted into the vector pFast Bac HTb to yield pFast Bac HTb CPα. Next, the RsrII GST RsrII fragment derived from pFast Bac HTb GST was inserted into pFast Bac HTb CPα to yield pFast Bac HTb GST CPα. pGBT9-Tctex-1 was used as a template to amplify the coding sequences for Tctex-1 with primers designed to introduce flanking EcoRI and SalI sites. The resulting product was inserted into the appropriately digested pFast Bac HTb CPα to yield pFast Bac (HTb) GST Tctex-1.

The GST fusion protein was expressed by baculovirus using the Fast-Bac system (Gibco-Invitrogen Co.). Sf-9 cells were infected with the virus in EX-CELL 400 medium (JRH Bioscience). The virus was harvested 72 h after infection and purified. The infected cells (5×10^7) were suspended in 1 ml of sonication buffer (50 mM NaCl, 1 mM EDTA, 1 mM phenylmethylsulfonyl fluoride, and protease inhibitors), and lysed by sonication. After the addition of 150 μl of Triton X-100, the lysates were rotated at 4°C for 20 min and centrifuged at 14,000 × *g* at 4°C for 30 min. The supernatant was filtered with a 0.45-μm-pore-size membrane filter and incubated with 150 μl of glutathione-Sepharose 4B beads [equilibrated in PBS(−)] at 4°C for 5 h. The beads were washed four times with ice-cold PBS(−) (with rotation for 10 min at 4°C for each wash).

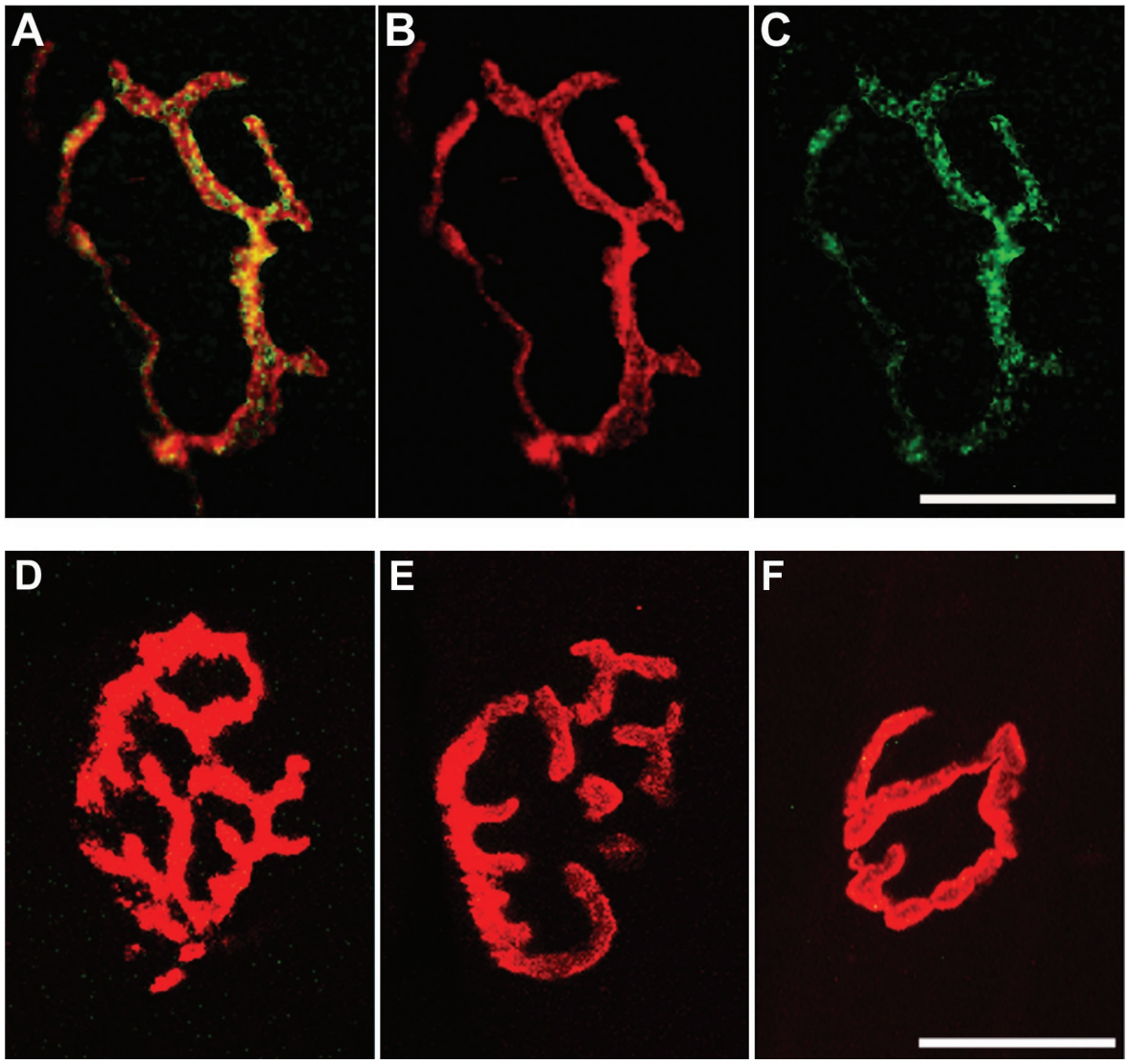

FIG. 1. PV localized at neuromuscular junctions in Tg mice. PV was i.m. injected into Tg mice, and the neuromuscular junctions were stained with α-bungarotoxin. To ascertain the point of injection under the stereoscope, Alexa Fluor 647-conjugated dextran 10,000 MW was coinjected with PV. The coinjection of PV with dextran did not reveal any difference from the injection of PV alone as far as the onset of initial paralysis was concerned. PV was immunostained with anti-PV antibodies and detected with fluorescein isothiocyanate-conjugated secondary antibodies. Panels A to C show the same specimen derived from a Tg mouse infected with PV. (B) α-Bungarotoxin. (C) PV. (A) Merged image of panels B and C. (D) Non-Tg mouse infected with PV. (E) Mock-infected Tg mouse. (F) Tg mouse infected with PV and immunostained without primary antibody. Bars, 20 μm.

GST-His_6-CPα and GST-His_6 were eluted with an elution buffer (20 mM reduced glutathione and 50 mM Tris-HCl [pH 8.0]). FLAG–Tctex-1 was separated from GST using Precision Protease (Amersham Biosciences) and collected. The purified protein was dissolved in HBS 2 (20 mM HEPES [pH 7.5] and 140 mM NaCl) using a VIVA SPIN column (VIVA Science). The purified proteins were analyzed by polyacrylamide gel electrophoresis (PAGE) and Coomassie brilliant blue (CBB) staining to check their purity.

GST pull down. GST fusion protein (50 μg) and glutathione-Sepharose 4B (10 μl as a bed volume) were mixed and incubated in a binding buffer (HBS 2 supplemented with 5 mM dithiothreitol and 0.1% Triton X-100) for 90 min at 4°C. The beads were washed four times with ice-cold binding buffer (with rotation for 10 min at 4°C for each wash).

For the binding assay, 100 ng of Tctex-1 was incubated with GST fusion protein bound to the 10-μl bed volume of glutathione-Sepharose 4B in a binding buffer for 30 min at 30°C, and the mixture was agitated every 5 min. The supernatant was removed, and a 20-μl bed volume of glutathione-Sepharose 4B was added. The beads were washed six times with ice-cold binding buffer. They were resuspended in 1× sample buffer (50 mM Tris-HCl [pH 6.7], 1.6% sodium dodecyl sulfate [SDS], 4% glycerol, 4% 2-mercaptoethanol, and 0.004% bromophenol blue), and then the eluted proteins were detected by Western blotting

FIG. 2. Electron microscopic images of nerve endings at the neuromuscular junctions of Tg mice after PV injection. (A) Epon-embedded nerve terminal of the neuromuscular junction of a Tg mouse after inoculation with PV. Bar, 1 μm. (B) Enlargement of the boxed area of the nerve terminal in panel A. PV virion-like particles in a vesicle are indicated by the arrow. Bar, 100 nm. (C) Ultracryoimmunogold labeling by anti-PV antibody. Several gold particles are found on vesicle-like structures (arrows) in nerve terminals. Bar, 100 nm.

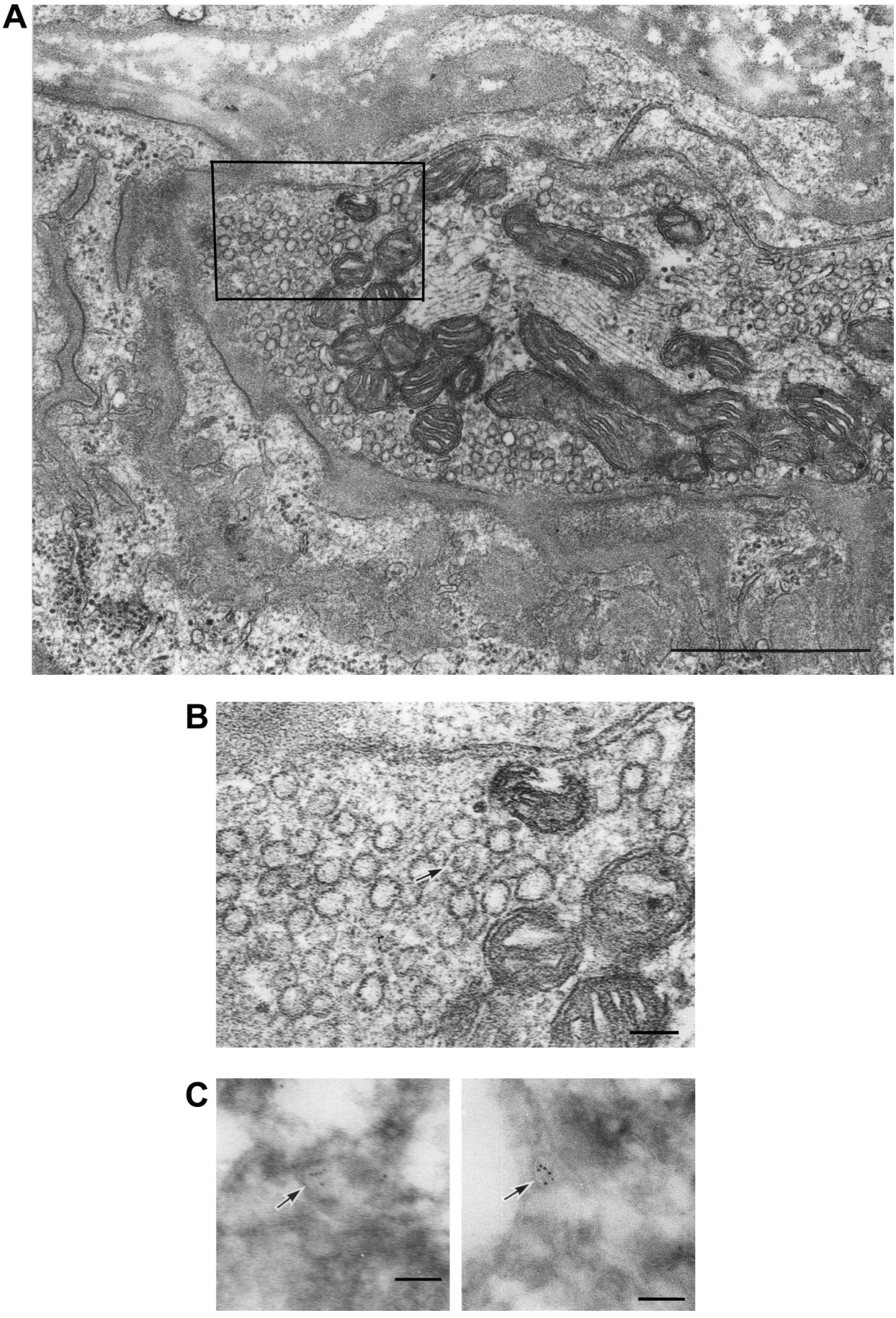
A
B
C

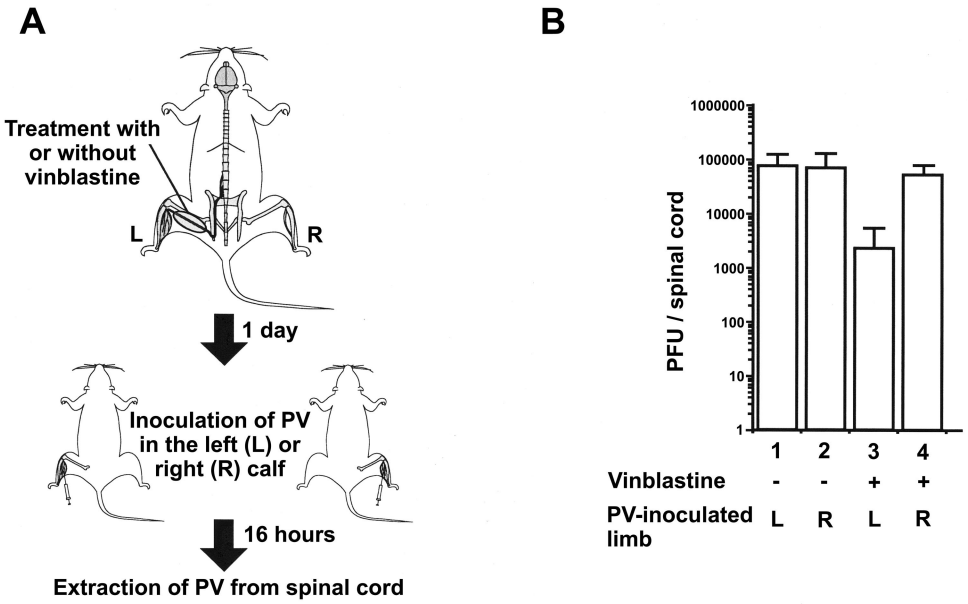

FIG. 3. Effect of vinblastine on axonal transport. (A) Method used for the experiment. The sciatic nerve of Tg mice was treated with PBS(−) with or without vinblastine. The next day, virus was inoculated into the left (L) or right (R) calf. Virus was then extracted from the spinal cord 16 h after the inoculation. (B) Amounts of PV detected in spinal cord by plaque assay. Three mice were used for each condition. +, present; −, absent.

with rabbit anti-FLAG M2 monoclonal antibody (MAb) (Sigma) after separation by SDS-PAGE.

Antibodies. Mouse anti-hPVR MAb, D171 (NeoMarkers), was used for immunostaining. For the detection of PV, rabbit anti-PV hyperimmune serum was used. When biotinilated anti-PV antibody was used, the rabbit anti-PV hyperimmune serum was purified with an Econo-Pac Protein A kit (Bio-Rad) and then biotinilated using a FluoReporter Biotin-XX protein labeling kit (Molecular Probes, Inc., Eugene, Oreg.). The anti-Tctex-1 polyclonal antibodies R5205 (provided by S. M. King [27]) were used for Western blotting and immunohistochemistry. As secondary antibodies, Alexa Fluor 488-conjugated goat anti-mouse IgG, Alexa Fluor 568-conjugated goat anti-rabbit IgG, Alexa Fluor 647-conjugated goat anti-rabbit IgG, and Alexa Fluor 568-conjugated streptavidin (Molecular Probes) were used.

Imaging. The differentiated PC12 cells on glass bottom dishes were incubated with 10^6 PFU of PV per well and 667 μg of tetramethylrhodamine-conjugated dextran 3000 MW/ml at 37°C for 15 min. After the incubation, the cells were washed three times with N_2 medium and incubated in a CO_2 chamber at 37°C on the stage of an upright microscope (Axio-phot; Zeiss). Time lapse images of the distribution and dynamics of fluorescent materials in PC12 cells were collected on a confocal laser scanning microscope (LSM510; Zeiss) (http://microbiology.m.u-tokyo.ac.jp/ohokamovie.htm).

Immunocytochemistry. The differentiated PC12 cells on glass bottom dishes were treated with 10^6 PFU of PV per well and 667 μg of tetramethylrhodamine-conjugated dextran 3000 MW/ml at 37°C for 30 min. The infected cells were then washed three times with N_2 medium, fixed in PBS(−) containing 2% paraformaldehyde for 15 min, and washed four times in PBS(−).

All the immunocytochemical reactions were carried out at RT unless otherwise specified. The fixed cells were incubated for 1 h with PBS(−) containing 0.05% saponin and 10% normal goat serum for permeation and blocking of nonspecific reactions. The fixed cells were incubated first with primary antibody for 2 h. After a wash in PBS(−), secondary antibodies were applied to the sections for 1.5 h. Between the incubation steps, the cells were extensively washed. The cells were mounted in 80% glycerol in buffered PBS(−) and imaged under a laser scanning microscope (LSM510).

Double labeling was performed for anti-PV and α-bungarotoxin (neuromuscular junctions). After fixation, muscles were dissected out and gently teased and processed for immunostaining. The teased muscles were blocked in 10% normal goat serum in 0.1 M Tris-buffered saline (TBS) (0.1 M Tris-HCl [pH 7.4] and 0.85% NaCl) for 2 h at RT and incubated with rabbit anti-PV antibodies (1:200 dilution) in TBS for 48 h at 4°C. After a wash with TBS, the specimens were incubated in fluorescein isothiocyanate-conjugated goat anti-rabbit IgG (Dako) (1:100 dilution) for 2 h at RT. Following several washes, the specimens were incubated for 30 min at RT in 5 μg of tetramethylrhodamine-conjugated α-bungarotoxin (Molecular Probes)/ml diluted in 1% bovine serum albumin in sterile lactated Ringer's solution.

Electron microscopy. The tibialis anterior muscle was injected with PV and 10 μg of Alexa Fluor 647-conjugated dextran 10,000 MW (Molecular Probes) per mouse. The tissue was dissected out 1.5 h after the injection and kept in the same fixative for 30 min at RT. After being washed with 0.1 M phosphate buffer (19 mM NaH_2PO_4 and 81 mM Na_2HPO_4 [pH 7.4]), the specimens were stained with rhodamine-conjugated α-bungarotoxin (Molecular Probes) for 30 min at RT. The area with neuromuscular junctions was trimmed under a fluorescent binocular microscope.

For ordinary electron microscopy, the trimmed specimens were transferred to a fixative containing 2% paraformaldehyde and 2.5% glutaraldehyde in 0.1 M phosphate buffer. The tissues were stored in the same fixative for 5 h. After osmification in a 1% osmium tetroxide solution, the specimens were dehydrated through a graded alcohol series and embedded in Epon 812. Ultrathin sections were cut on an Ultracut microtome (Reichert) and stained with uranyl acetate and lead citrate. The sections were observed under an electron microscope (Hitachi H-7100).

For ultracryoimmunohistochemistry, trimmed specimens washed with 0.1 M phosphate buffer were infused with a mixture of 20% polyvinylpyrrolidone and processed for ultracryotomy on an Ultracut microtome equipped with FCS (Reichert) following the method of Tokuyasu (39). Briefly, sections of frozen specimens were collected with drops of 2.3 M sucrose, placed on a grid, and thawed at RT. After being blocked with 10% normal goat serum, the sections were incubated in TBS containing a 1:200 dilution of anti-PV hyperimmune serum for 24 to 48 h at 4°C and then washed with TBS and incubated with goat anti-rabbit IgG antibodies conjugated with 5- or 10-nm-diameter gold particles (Amersham) for 2 h at RT. Thereafter, the sections were rinsed and embedded with a mixture of 1% polyvinyl alcohol containing 0.1% uranyl acetate and observed under an electron microscope (Hitachi H-7100) after drying.

RESULTS

PV endocytosis at neuromuscular junctions of the Tg mouse. PV is transported retrogradely by the fast axonal transport system, and PV antigen is detected inside axons (35). However, it is still unclear whether PV is enclosed in vesicles during its

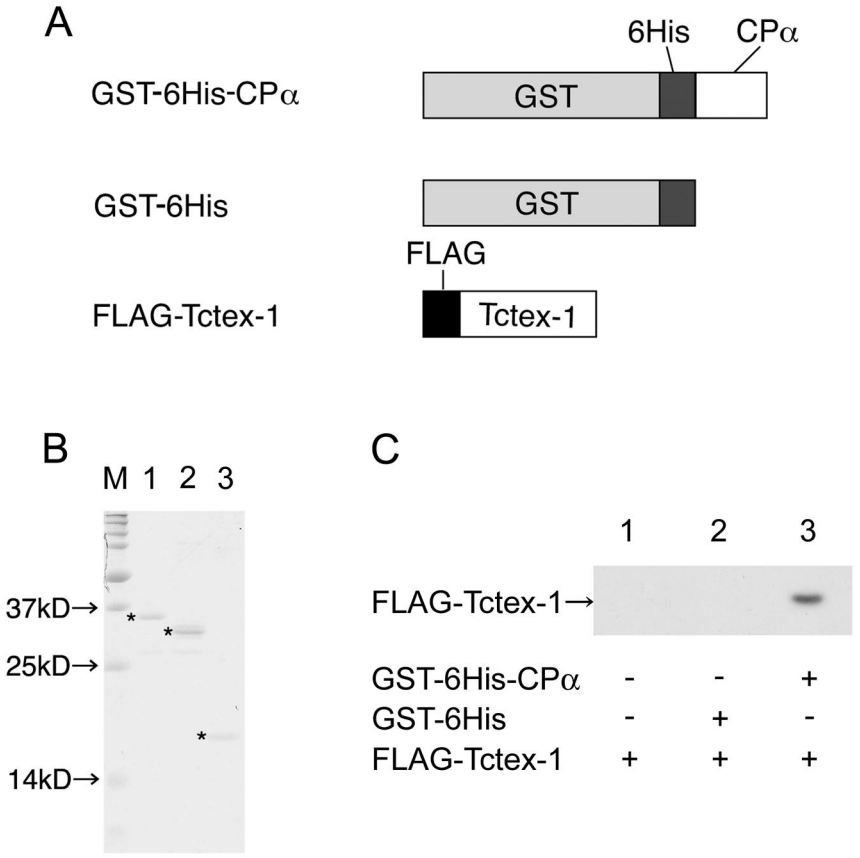

FIG. 4. Direct interaction between hPVR CP and Tctex-1. Purified proteins were subjected to GST pull down. (A) Structures of purified proteins used. (B) CBB staining of purified proteins. M, molecular mass markers. The asterisks indicate intact purified proteins. Lane 1, GST-His_6-CPα; lane 2, GST-His_6; lane 3, FLAG–Tctex-1. (C) GST pull-down analysis of purified proteins. Lane 1, FLAG–Tctex-1 only (+); lane 2, GST-His_6 and FLAG–Tctex-1; lane 3, GST-His_6-CPα and FLAG–Tctex-1.

transport, although vesicles are known to be conveyed by the fast axonal transport system (6). To examine whether PV is incorporated into neurons at nerve terminals, immunohistochemistry was employed to clarify the localization of PV at neuromuscular junctions. As shown in Fig. 1, i.m.-inoculated PV was detected specifically at neuromuscular junctions of Tg mice stained with tetramethylrhodamine-conjugated α-bungarotoxin, a specific marker of neuromuscular junctions. I.m.-inoculated PV was not detected in a similar region in non-Tg mice. This result suggests that PV is incorporated into nerve terminals at neuromuscular junctions, depending on hPVR.

To elucidate whether synapses at neuromuscular junctions incorporate PV as vesicles, neuromuscular junctions after the inoculation of PV were closely observed under an electron microscope (Fig. 2A and B) and an immunoelectron microscope (Fig. 2C). PV antigens were reacted with rabbit anti-PV hyperimmune antibodies, and the antibodies were detected using goat anti-rabbit IgG antibodies conjugated with gold particles. As shown in Fig. 2C, gold particles were found on vesicle structures in nerve terminals of neuromuscular junctions. A similar vesicle (Fig. 2B) appeared to contain several PV virions, considering the area of scattered virus-like particles. These results strongly support the notion that PV is incorporated into vesicles at the nerve terminals.

Microtubule dependency of the fast retrograde axonal transport of PV. The fast retrograde transport system is thought to be associated with microtubules (6). Accordingly, the involvement of microtubules in the transport of PV was investigated. Vinblastine, known as an inhibitor of tubulin polymerization and used to inhibit axonal transport in vivo (7, 11, 42, 45), was employed to treat the sciatic nerve to examine whether microtubules are involved in transport (Fig. 3A). The left sciatic nerve of PV-sensitive Tg mice was treated with vinblastine in PBS(−) (Fig. 3A). As a control, PBS(−) without vinblastine was used. One day after the treatment, the mice were inoculated with 10^6 PFU of PV injected into the left or right calf. Tissue samples of the spinal cord were prepared from 16 h postinoculation until the time that replication of PV must have begun in the spinal cord (35), and virus titers from the tissue samples were measured (Fig. 3B). In the spinal cords of the PBS(−)-treated mice inoculated with virus in the same (left) or opposite (right) side, $\sim 7 \times 10^4$ PFU of virus was detected. The data suggest that the treatment of the sciatic nerve with PBS(−) had no effect on the efficiency of axonal transport of PV. When the mice treated with vinblastine were inoculated with virus in the opposite (right) side, $\sim 5 \times 10^4$ PFU of the virus was detected in the spinal cord. This suggests that treatment with vinblastine had little influence on the replication of

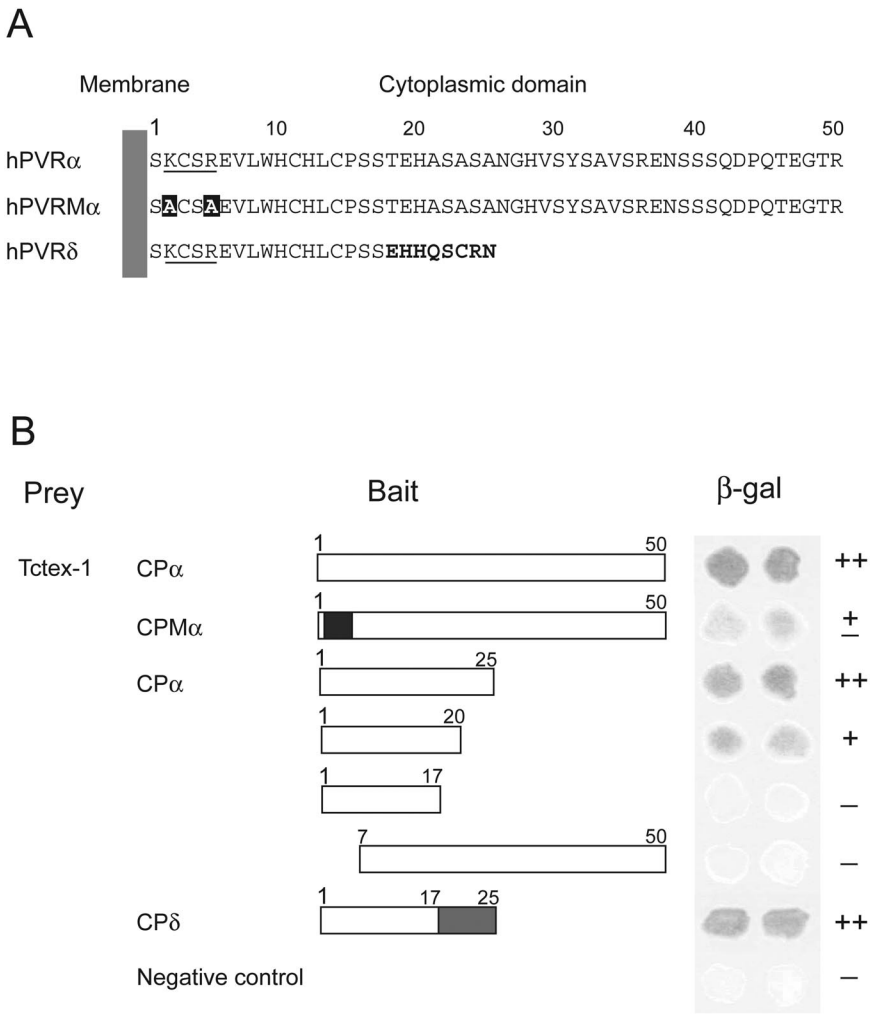

FIG. 5. Interaction between truncated hPVR CPs and Tctex-1. Using yeast two-hybrid analysis, interactions between Tctex-1 and the truncated proteins were investigated. (A) Amino acid sequences in hPVR CPs. The numbers above the sequences indicate the amino acid numbers in the hPVR CPs. The consensus sequences proposed for Tctex-1 interaction are underlined. The substituted amino acids are in solid boxes. The residues of hPVRδ shown in boldface differ from those in hPVRα. (B) Solid boxes, substituted amino acid residues in the consensus sequence for Tctex-1 interaction; shaded boxes, amino acid sequences different from that of CPα. β-Galactosidase activity was examined using the β-galactosidase filter assay. The activity is shown with a plus or minus sign on the right: ++, strong; +, intermediate; ±, weak; −, undetectable interaction. A strain transformed with pPC97 and pPC86 was used as the no-interaction control.

virus in the spinal cord. On the other hand, in the spinal cords of the mice treated with vinblastine and inoculated with virus in the same (left) side, only $\sim 2 \times 10^3$ PFU was detected. These results indicate that vinblastine treatment greatly reduced the efficiency of the axonal transport of PV through the sciatic nerve, suggesting that microtubules are part of the transport system. As it is known that the cytoplasmic dynein motor protein moves retrogradely along microtubules, the participation of microtubules implies that cytoplasmic dynein is involved in the transport of PV-containing substances.

Direct interaction of hPVR CP with Tctex-1. It has been reported that hPVR CP associates with Tctex-1, a subunit of the dynein complex (31, 33). In addition, PVs are actually incorporated into vesicles at nerve terminals, as demonstrated in Fig. 1 and 2. Thus, it seems that PV-containing vesicles are transported with the aid of interaction between hPVR CP and dynein.

To clarify whether the hPVR CP directly binds Tctex-1, purified recombinants of these proteins were employed in GST pull-down experiments. GST, His_6, and FLAG were used as tags for CPα and Tctex-1. The structures of recombinant proteins used in the binding assay are shown in Fig. 4A. All of the proteins were produced by a baculovirus expression system and purified using a glutathione-Sepharose 4B column. GST-FLAG-tagged Tctex-1 was digested with Precision protease at the junction between GST and FLAG, and the FLAG-tagged Tctex-1 moiety (FLAG–Tctex-1) was isolated. GST-His_6 was used as a control. Affinity-purified recombinant proteins were analyzed by PAGE followed by CBB staining. As shown in Fig. 4B, recombinant proteins were highly purified, although some degradation products were seen. Purified FLAG–Tctex-1 was mixed with purified GST-His_6-tagged CPα (GST-His_6-CPα) or GST-His_6 bound to glutathione-Sepharose 4B beads. After a wash, the proteins bound to the beads were separated by

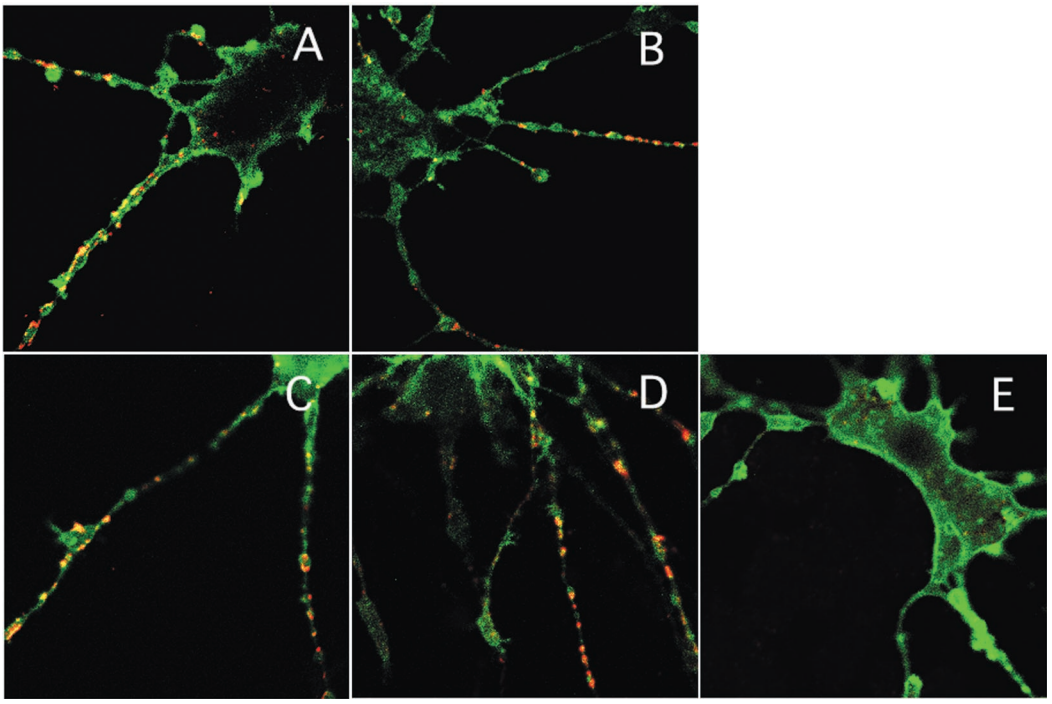

FIG. 6. Localization of hPVRs in PC12 cells. hPVRα (A and E), hPVRMα (B), hPVRα-GFP (C), and hPVRMα-GFP (D) were introduced into PC12 cells. (A to D) The cells were incubated with PV. The cells transfected with hPVRα (A and E) or hPVRMα (B) were immunostained with anti-hPVR and anti-PV antibodies. These primary antibodies were stained with Alexa Fluor 488 (green)-conjugated antibody and Alexa Fluor 568 (red)-conjugated antibody, respectively. In the case of hPVRα-GFP (C) and hPVRMα-GFP (D), cells were incubated with only anti-PV antibody and detected using Alexa Fluor 568 (red)-conjugated antibody.

PAGE in the presence of SDS and visualized by Western blotting using rabbit anti-Tctex-1 antibodies (R5205). As shown in Fig. 4C, FLAG–Tctex-1 was coprecipitated with GST-His_6-CPα but not with GST-His_6. Approximately 2 to 5% of FLAG–Tctex-1 was precipitated with GST-His_6-CPα under the conditions described in Materials and Methods. These results indicate that Tctex-1 interacts directly with CPα.

Amino acid sequences required for interaction between Tctex-1 and hPVR CP. To identify the region of CPα which interacts with Tctex-1, a truncation analysis was performed using the yeast two-hybrid system. A series of deletion mutants of CP were prepared as described in Materials and Methods. The structures of these mutants are shown in Fig. 5B. The region encompassing aa 1 to 25 shows an almost complete ability to interact with Tctex-1, aa 1 to 20 shows a reduced ability compared with aa 1 to 25, and aa 1 to 17 shows no ability. Deletion of six N-terminal amino acid residues, including the consensus sequence KXXR for Tctex-1 binding, abrogates the interaction with Tctex-1. These results suggest that the N-terminal 25-aa sequence of CPα is required for efficient interaction.

As for hPVRδ, whole CP showed an ability to interact with Tctex-1. This result indicates that CPδ, as well as CPα, interacts with Tctex-1. Since the N-terminal 17-aa sequence common to hPVRα and hPVRδ is not sufficient for binding to Tctex-1, several or all of the amino acids from aa 18 to 25 of CPδ are also required for the interaction.

To clarify the contribution of the KXXR consensus sequence to the binding of Tctex-1, alanine substitutions were introduced into the KXXR sequence of an intact CPα. The AXXA mutant (CPMα) apparently showed less β-galactosidase activity than the intact CPα (Fig. 5B). This result suggests that KXXR significantly contributes to the interaction, although it is not the only determinant for Tctex-1 binding.

Functions of mutant PVRs in PC12 cells. To observe the localization of hPVR-containing vesicles in the axons of live neural cells, differentiated rat PC12 cells were employed. PC12 cells are well known as a neural-axon model that expresses Tctex-1 (26) and does not express hPVR naturally. PC12 cells were transfected with a vector for the expression of hPVRα, hPVRMα (a mutant hPVR carrying CPMα), GFP-tagged hPVRα (hPVRα-GFP), or GFP-tagged hPVRMα (hPVRMα-GFP). All of these hPVRs were successfully expressed in PC12 cells (Fig. 6) and conferred permissiveness for infection (data not shown). As shown in Fig. 6, PV antigens were detected in regions where hPVRs were detected in PC12 cells infected with PV. The data indicate that alanine substitutions in the KXXR sequence and the GFP tag do not seriously affect the function of hPVR in terms of PV infection and that PV antigens colocalize with hPVRs in PC12 cells. No PV was detected in PC12 cells which did not express hPVRs (data not shown). The results are consistent with the observation that PV is incorporated into the cells by hPVR-mediated endocytosis (Fig. 1).

Interaction of hPVRs with Tctex-1 in PC12 cells. To examine the contribution of the interaction between hPVR CP and Tctex-1 to the colocalization of PV, hPVR, and Tctex-1 in PC12 cells, an immunocytochemical technique was employed to observe the infected PC12 cells expressing various hPVRs. As shown in Fig. 7A, PV-containing vesicles with hPVRα-GFP

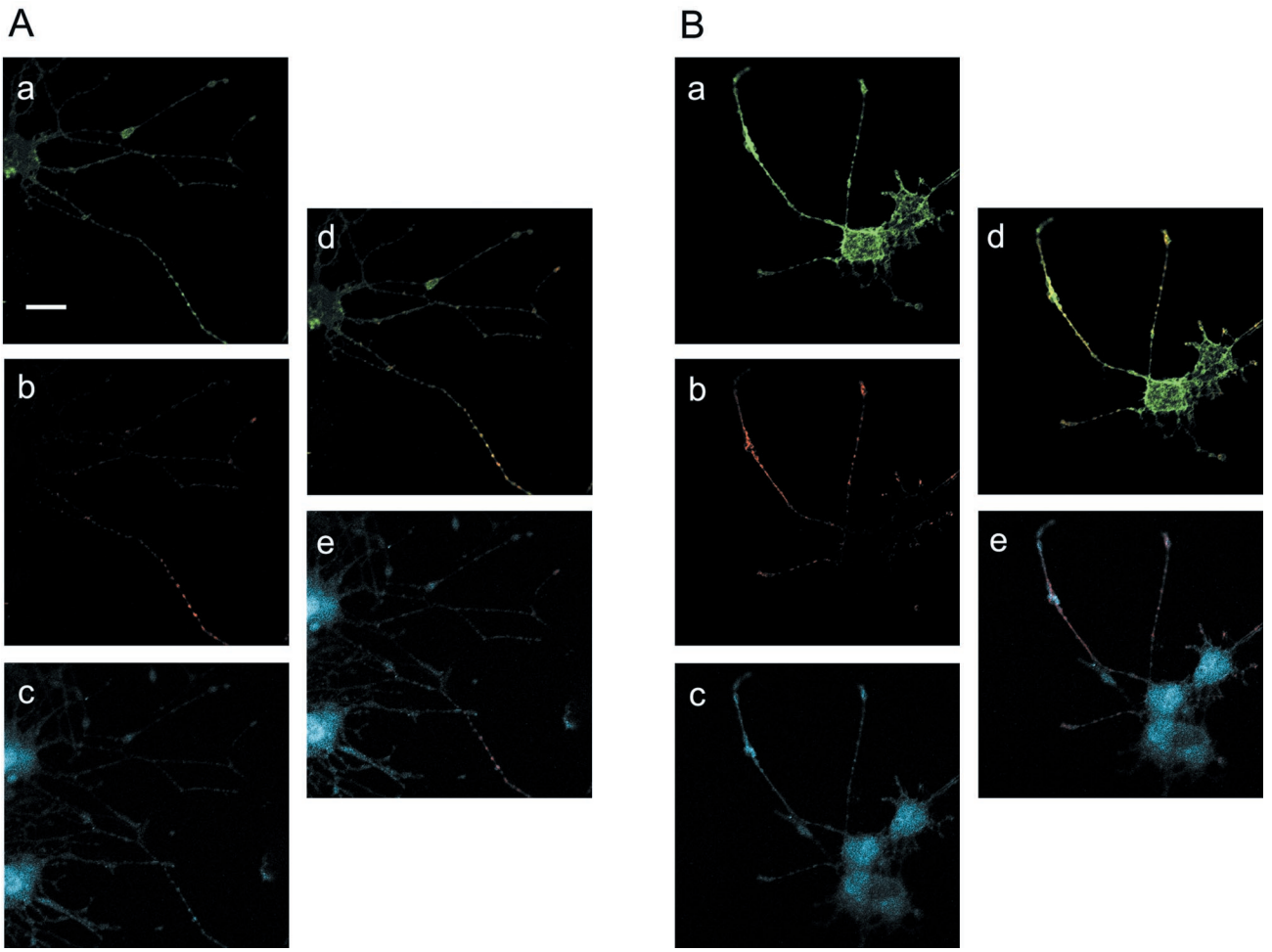

FIG. 7. PV, hPVRs, and Tctex-1 colocalized in PC12 cells. PC12 cells transfected with hPVRα-GFP (A) or hPVRMα-GFP (B) were incubated with PV and fixed. Immunofluorescence microscopy was performed using specific antibodies, that is, biotinylated rabbit anti-PV antibodies and rabbit anti-Tctex-1 antibodies (R5205). hPVRs were detected as enhanced GFP autofluorescence. (a and d) hPVRs; (b, d, and e) PV; (c and e) Tctex-1. Bar, 20 μm.

colocalized with Tctex-1 in axons. These results support the notion that PV-containing vesicles with hPVRα-GFP are transported by cytoplasmic dynein in axons of PC12 cells. As to PV-containing vesicles with hPVRMα-GFP (Fig. 7B), no obvious difference in colocalization with Tctex-1 was observed compared to the vesicles with hPVRα-GFP, although CPMα has less ability to interact with Tctex-1 than CPα, as shown in Fig. 5. Thus, immunocytochemical data comparable to those from the yeast two-hybrid assay were not obtained. A possible reduced affinity of hPVRMα for Tctex-1 might be enough for these molecules to colocalize in vivo.

The colocalization of hPVRα- and hPVRMα-containing endosomes with PV was carefully examined to elucidate any difference in the characters of these hPVRs. Tetramethylrhodamine-conjugated dextran was used as an endosomal marker (25). To prove that the vesicles with hPVR and dextran really contain PV, PC12 cells were transfected with expression vectors for GFP-tagged hPVRs, differentiated, and incubated with PV and dextran at 37°C for 30 min for immunocytochemistry. In hPVRα-GFP-expressing cells, vesicles containing hPVRα and dextran always colocalized with PV (Fig. 8A [a to d] and B [a]). Vesicles containing only hPVRα or only dextran also existed. In hPVRMα-GFP-expressing cells, similar results were obtained (Fig. 8A [e to h] and B). These findings indicate that hPVR-containing endosomes always contain PV. Thus, we were unable to distinguish between hPVRα and hPVRMα in regard to colocalization with Tctex-1. However, this observation makes it possible to investigate the movement of PV-containing vesicles in axons of PC12 cells by monitoring the movement of dextran with hPVRs in the infected cells, although it is impossible to observe PV particles directly in live cells at present.

Axonal transport of vesicles containing hPVRs, followed by PV infection. Movements of vesicles containing hPVRs and dextran were observed in PC12 cells after PV infection. When PV and dextran were applied to hPVRα-GFP-expressing cells, all the vesicles containing both hPVRα-GFP and dextran displayed retrograde transport, and none of them showed anterograde transport (Fig. 9A). This suggests that hPVRα is retrogradely transported with PV, as well as dextran, in the axons of PC12 cells. The average transport velocity of vesicles containing both hPVRα-GFP and dextran was ~0.4 μm/s. The trans-

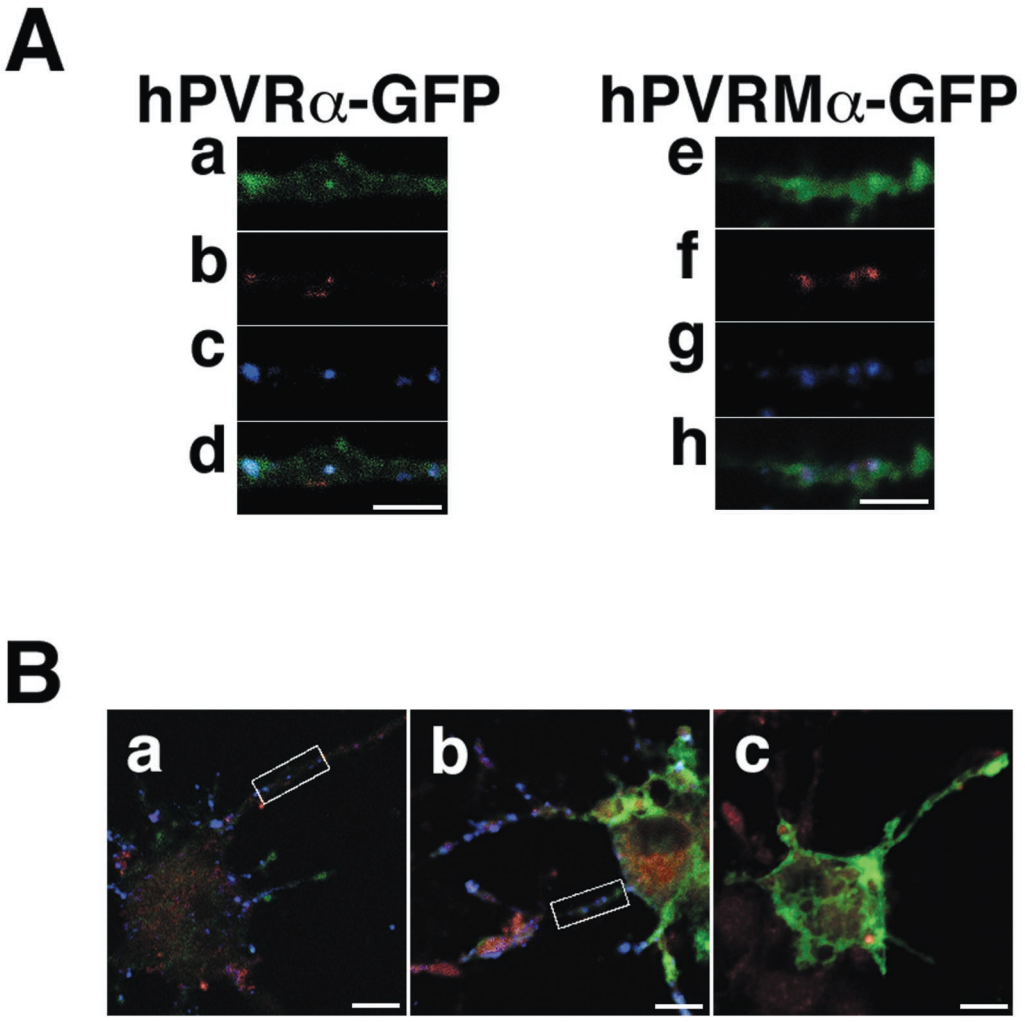

FIG. 8. Vesicles containing both hPVRs and dextran colocalize with PV in PC12 cells. (A) PC12 cells transfected with hPVRα-GFP (a to d) or hPVRMα-GFP (e to h) were incubated with PV and tetramethylrhodamine-conjugated dextran and then fixed. The cells were immunostained with anti-PV primary antibodies and Alexa Fluor 647-conjugated secondary antibodies. Green shows the localization of hPVRs (a and e), red shows the localization of dextran (b and f), and blue shows the localization of PV (c and g). (d and h) Merged images. Bars, 5 μm. (B) Wide view of immunostained PC12 cells. The boxed portions are magnified in panel A. PC12 cells were transfected with hPVRα-GFP (a) or hPVRMα-GFP (b and c). The cells were incubated with tetramethylrhodamine-conjugated dextran (a to c) and with (a and b) or without (c) PV. Bars, 10 μm.

port was inhibited by treatment with colchicines, an inhibitor for tubulin polymerization (data not shown). PV incorporation was inhibited by adding the anti-hPVR MAb p286 (data not shown).

To examine the importance of the KXXR consensus sequence to the retrograde transport of hPVR-containing endosomes in PC12 cells infected with PV, the vesicle transport in hPVRMα-GFP-expressing cells was observed. When PV and dextran were added to the hPVRMα-GFP-expressing cells, individual vesicles containing both hPVRMα and dextran moved anterogradely (72%) or retrogradely (28%) (Fig. 9C). The average velocity of vesicles containing both hPVRMα-GFP and dextran was ~0.4 μm/s for the anterograde transport and ~0.5 μm/s for the retrograde transport. Thus, the directions of transportation of vesicles containing hPVRMα and dextran differ in individual vesicles. The data indicate that the consensus sequence for the interaction of Tctex-1 with CPα is important for retrograde transport of hPVRα, dextran, and PV. Perhaps an efficient interaction of hPVR with Tctex-1 is required for the efficient retrograde transport of PV.

DISCUSSION

The results presented here have clarified several unknown features of axonal transport of PV, namely, (i) the existence of PV-containing vesicles in neurons at neuromuscular junctions, (ii) direct interaction of CPα with Tctex-1, and (iii) the importance of efficient interaction between Tctex-1 and CPα for retrograde transport of PV-containing vesicles. As a result, one can have more confidence in previously presumed mechanisms for the axonal transport of PV.

It has been reported that PV enters HeLa cells by receptor-mediated endocytosis as an intact infectious particle, viruses are enclosed in clathrin-coated vesicles 10 min after adsorption, and intact viral particles can be recovered from the cells for up to 30 min after adsorption (Fig. 10B) (43). However,

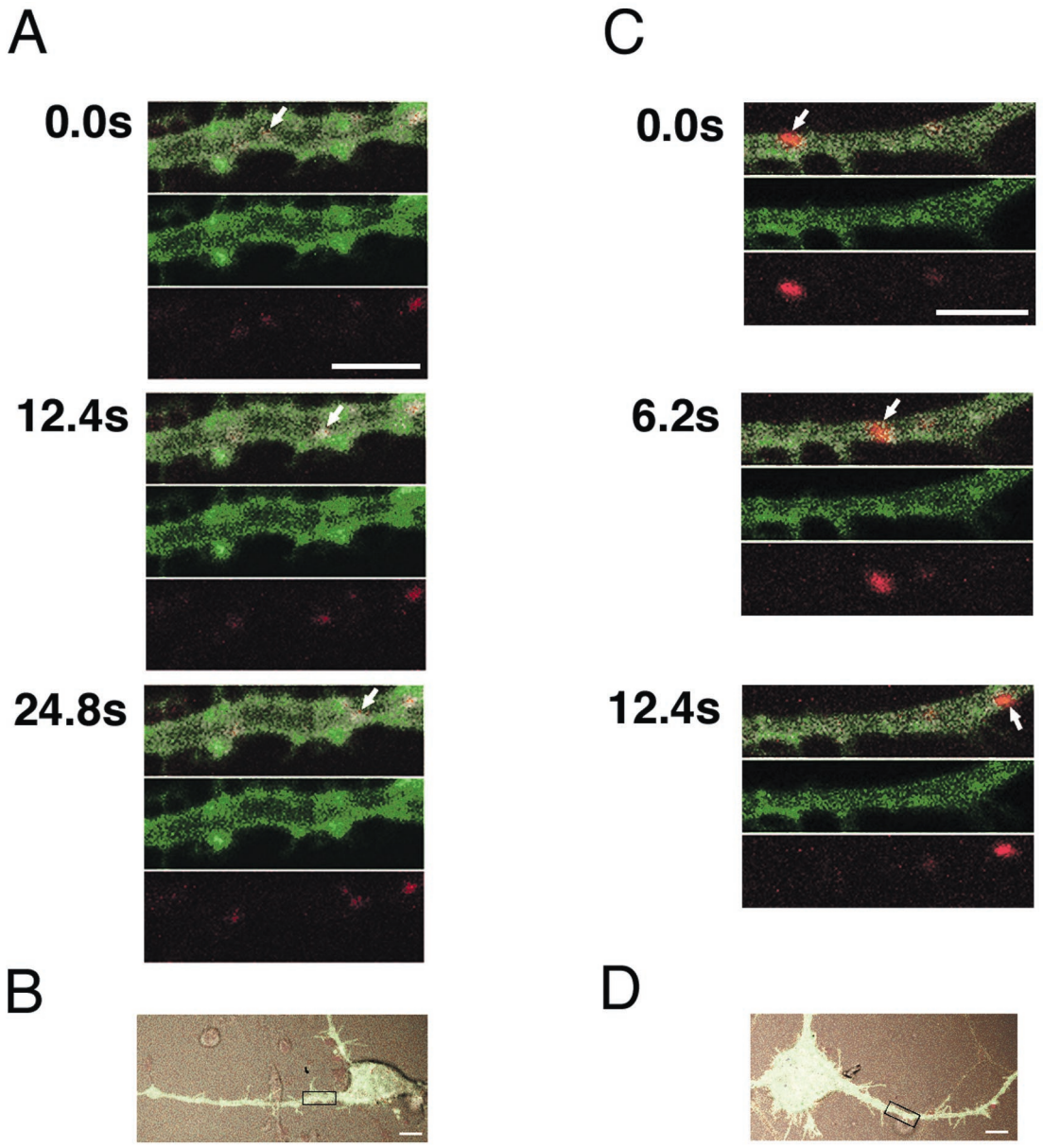

FIG. 9. Axonal transport of hPVRα-GFP or hPVRMα-GFP-expressing vesicles in PC12 cells. PC12 cells transfected with hPVRα-GFP (A and B) or hPVRMα-GFP (C and D) were incubated with tetramethylrhodamine-conjugated dextran and PV and subjected to video rate scanning under a confocal microscope. The boxed areas in panels B and D were magnified and observed. Red shows the localization of dextran, and green shows the localization of hPVRs. The uppermost images at each time point are merged. The arrows indicate the vesicles containing dextran and hPVRs. Bars, 5 (A and C) and 10 (B and D) μm.

DeTulleo and Kirchhausen (10) found by using a dominant-negative mutant of dynamin that PV might not require the clathrin pathway. Moreover, an alternate system of endocytosis has been shown to be induced in cells expressing dominant-negative dynamin (9). Thus, the mechanisms for PV endocytosis are still controversial.

There is a consistent argument for the penetration by PV of cultured cells, that is, fusion occurring between PV particles and the surface membranes of cells (Fig. 10A) (8). In this pathway, only RNA enters the host cell's cytoplasm. There might be multiple pathways by which PV penetrates cultured cells (Fig. 10) (2). As to the penetration at synapses, it has been thought that endocytosis is the main pathway, since we have shown that intact PV particles are recovered from axons of the sciatic nerve of Tg mice inoculated with PV in the calf. Fusion at synapses might also be possible and result in the long-distance transport of uncoated PV RNA through axons. Indeed, it has recently been reported that PV replicon RNA is transported from neuromuscular junctions to the neural-cell body (22). After the transportation of PV through axons, replication occurs in the neural-cell body, where uncoating might occur via a fusion pathway in particular endosomes (Fig. 10C). Much work remains to be done to elucidate the mechanisms by which PV replication starts in the cell body.

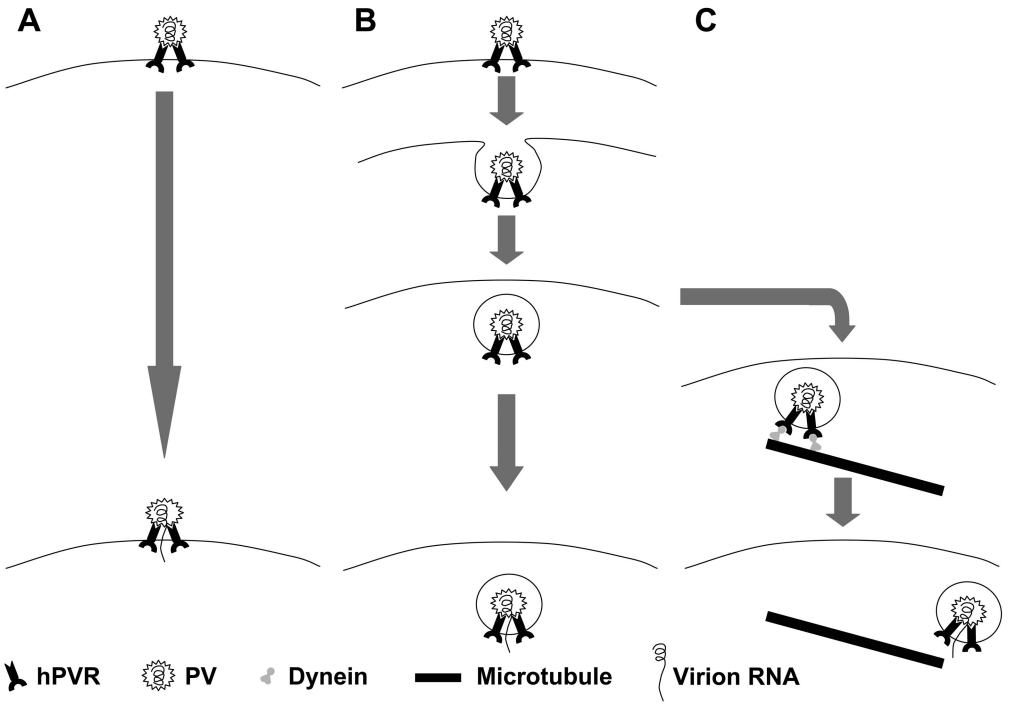

FIG. 10. Hypothesis for mechanisms of early infection of PV. (A) PV interacts with hPVR and fuses with the lipid bilayer on the cellular membrane, and then the viral genomic RNA transfers into the cytoplasm. This is mainly observed in HeLa cells (8). (B) PV adheres to hPVR and is incorporated into endosomes. The pH or other factors inside the endosomes might make PV unstable and cause the release of its genomic RNA into the cytoplasm. This is also observed in HeLa cells (43). (C) PV adheres to hPVR and is incorporated into endosomes. The endosomes are transported by dynein along microtubules, and the viral genomic RNA transfers into the cytoplasm. PV fuses with the lipid bilayer on the endosomal membrane under particular conditions. This possibly occurs in HeLa cells, as well as neural cells.

It is interesting that individual hPVRMα-containing vesicles move retrogradely or anterogradely, whereas hPVRα-containing vesicles only move retrogradely. This observation suggests that the surfaces of hPVRMα (or hPVRα)-containing vesicles carry other molecules that have affinity for motor molecules for anterograde transport. Since CPMα has less affinity than CPα for Tctex-1, the movement of hPVRMα-containing vesicles may be influenced more by other molecules on the surfaces of endosomes. The population and types of such surface molecules may determine the direction of movement of individual vesicles in the axon. It should be noted that no vesicles moved both retrogradely and anterogradely under the conditions used.

The average transport velocity of hPVRα-containing vesicles with PV in the axons of PC12 cells was estimated to be 0.4 μm/s (3.5 cm/day), which is much slower than that observed in the sciatic nerve of the Tg21 mouse (35). A similar phenomenon was reported for axonal transport of TrkA, a receptor for NGF, in the axons of PC12 cells. The retrograde transport velocity of TrkA was measured at 0.3 ± 0.05 μm/s in PC12 cells (15), although NGF is transported by a fast retrograde transport system in the sciatic nerve in vivo, like PV. The reason for the slow transportation in PC12 cells is not known at present. However, it is possible that transport velocities vary in individual cells and tissues because of different populations of motor molecules in different transport systems.

Both hPVRα and hPVRδ must be active for PV to be transported, according to the result of the yeast two-hybrid assay involving Tctex-1 and hPVR CP (Fig. 5). In polarized cells, hPVRα is expressed on the basolateral surface and hPVRδ is expressed on both the apical and basolateral surfaces. It would be interesting to know which and how much hPVR is expressed at synapses. However, to date, we have been unable to detect hPVRs using any anti-hPVR antibodies in the sciatic nerve of the Tg21 mouse model. Thus, the expression level of hPVRs is probably very low in this tissue. Although it is not known how much hPVR is necessary for the incorporation of PV into endosomes, hPVR plays an important role in incorporation at synapses, because the process is inhibited by the anti-hPVR MAb p286, which binds to the N-terminal Ig-like domain of hPVRs and is able to block PV infection.

ACKNOWLEDGMENTS

We are grateful to T. Matano and H. Ohno for helpful suggestions and discussions. We thank K. Ishida and S. Hayashi, Iwate Medical University, for their excellent technical support. We also thank Y. Sasaki and H. Igarashi for expert technical assistance and E. Suzuki and Y. Matsushita for help in preparation of the manuscript.

This work was supported in part by Grants-in-Aid for Advanced Medical Science Research by the Ministry of Science, Education, Sports and Culture, Japan; Industrial Technology Research Grant Program in '02 from New Energy and Industrial Technology Development Organization (NEDO) of Japan; and a grant from the Ministry of Health and Welfare of Japan.

REFERENCES

1. **Aniento, F., N. Emans, G. Griffiths, and J. Gruenberg.** 1993. Cytoplasmic dynein-dependent vesicular transport from early to late endosomes. J. Cell Biol. **123:**1373–1387.
2. **Arita, M., S. Ohka, Y. Sasaki, and A. Nomoto.** 1999. Multiple pathways for establishment of poliovirus infection. Virus Res. **62:**97–105.
3. **Ausbel, I., and M. Frederick (ed.).** 2003. Chapter 20, unit 20.1: basic protocol

1. *In* Current protocols in molecular biology. John Wiley & Sons, Inc., New York, N.Y.
4. **Ausbel, I., and M. Frederick (ed.).** 2000. Current protocols in molecular biology, vol. 3, p. 13.1. John Wiley & Sons, Inc., New York, N.Y.
5. **Bottenstein, J. E., and G. H. Sato.** 1979. Growth of a rat neuroblastoma cell line in serum-free supplemented medium. Proc. Natl. Acad. Sci. USA **76:** 514–517.
6. **Brady, S. T.** 1991. Molecular motors in the nervous system. Neuron **7:**521–533.
7. **Bulenga, G., and T. Heaney.** 1978. Post-exposure local treatment of mice infected with rabies with two axonal flow inhibitors, colchicine and vinblastine. J. Gen. Virol. **39:**381–385.
8. **Curry, S., M. Chow, and J. M. Hogle.** 1996. The poliovirus 135S particle is infectious. J. Virol. **70:**7125–7131.
9. **Damke, H., T. Baba, A. M. van der Bliek, and S. L. Schmid.** 1995. Clathrin-independent pinocytosis is induced in cells overexpressing a temperature-sensitive mutant of dynamin. J. Cell Biol. **131:**69–80.
10. **DeTulleo, L., and T. Kirchhausen.** 1998. The clathrin endocytic pathway in viral infection. EMBO J. **17:**4585–4593.
11. **Fitzgerald, M., C. J. Woolf, S. J. Gibson, and P. S. Mallaburn.** 1984. Alterations in the structure, function, and chemistry of C fibers following local application of vinblastine to the sciatic nerve of the rat. J. Neurosci. **4:**430–441.
12. **Freistadt, M. S., and V. R. Racaniello.** 1991. Mutational analysis of the cellular receptor for poliovirus. J. Virol. **65:**3873–3876.
13. **Greene, L. A., and A. S. Tischler.** 1976. Establishment of a noradrenergic clonal line of rat adrenal pheochromocytoma cells which respond to nerve growth factor. Proc. Natl. Acad. Sci. USA **73:**2424–2428.
14. **Gromeier, M., and E. Wimmer.** 1998. Mechanism of injury-provoked poliomyelitis. J. Virol. **72:**5056–5060.
15. **Hirashima, N., M. Nishio, and M. Nakanishi.** 2000. Intracellular dynamics of a high affinity NGF receptor TrkA in PC12 cell. Biol. Pharm. Bull. **23:**1097–1099.
16. **Hirokawa, N.** 1998. Kinesin and dynein superfamily proteins and the mechanism of organelle transport. Science **279:**519–526.
17. **Hirokawa, N., Y. Noda, and Y. Okada.** 1998. Kinesin and dynein superfamily proteins in organelle transport and cell division. Curr. Opin. Cell Biol. **10:**60–73.
18. **Holzbaur, E. L., and R. B. Vallee.** 1994. Dyneins: molecular structure and cellular function. Annu. Rev. Cell Biol. **10:**339–372.
19. **Horie, H., S. Koike, T. Kurata, Y. Sato-Yoshida, I. Ise, Y. Ota, S. Abe, K. Hioki, H. Kato, C. Taya, et al.** 1994. Transgenic mice carrying the human poliovirus receptor: new animal models for study of poliovirus neurovirulence. J. Virol. **68:**681–688.
20. **Howe, H., and D. Bodian.** 1942. Neuronal mechanisms in poliomyelitis. Commonwealth Fund, New York, N.Y.
21. **Ito, H., Y. Fukuda, K. Murata, and A. Kimura.** 1983. Transformation of intact yeast cells treated with alkali cations. J. Bacteriol. **153:**163–168.
22. **Jackson, C. A., J. Messinger, M. T. Palmer, J. D. Peduzzi, and C. D. Morrow.** 2003. Gene expression in the muscle and central nervous system following intramuscular inoculation of encapsidated or naked poliovirus replicons. Virology **314:**45–61.
23. **Kashiba, H., E. Senba, Y. Kawai, Y. Ueda, and M. Tohyama.** 1992. Axonal blockade induces the expression of vasoactive intestinal polypeptide and galanin in rat dorsal root ganglion neurons. Brain Res. **577:**19–28.
24. **Katoh-Semba, R., S. Kitajima, Y. Yamazaki, and M. Sano.** 1987. Neuritic growth from a new subline of PC12 pheochromocytoma cells: cyclic AMP mimics the action of nerve growth factor. J. Neurosci. Res. **17:**36–44.
25. **Kauppi, M., A. Simonsen, B. Bremnes, A. Vieira, J. Callaghan, H. Stenmark, and V. M. Olkkonen.** 2002. The small GTPase Rab22 interacts with EEA1 and controls endosomal membrane trafficking. J. Cell Sci. **115:**899–911.
26. **King, S. M., E. Barbarese, J. F. Dillman III, S. E. Benashski, K. T. Do, R. S. Patel-King, and K. K. Pfister.** 1998. Cytoplasmic dynein contains a family of differentially expressed light chains. Biochemistry **37:**15033–15041.
27. **King, S. M., J. F. Dillman III, S. E. Benashski, R. J. Lye, R. S. Patel-King, and K. K. Pfister.** 1996. The mouse t-complex-encoded protein Tctex-1 is a light chain of brain cytoplasmic dynein. J. Biol. Chem. **271:**32281–32287.
28. **Koike, S., H. Horie, I. Ise, A. Okitsu, M. Yoshida, N. Iizuka, K. Takeuchi, T. Takegami, and A. Nomoto.** 1990. The poliovirus receptor protein is produced both as membrane-bound and secreted forms. EMBO J. **9:**3217–3224.
29. **Koike, S., I. Ise, and A. Nomoto.** 1991. Functional domains of the poliovirus receptor. Proc. Natl. Acad. Sci. USA **88:**4104–4108.
30. **Koike, S., C. Taya, T. Kurata, S. Abe, I. Ise, H. Yonekawa, and A. Nomoto.** 1991. Transgenic mice susceptible to poliovirus. Proc. Natl. Acad. Sci. USA **88:**951–955.
31. **Mueller, S., X. Cao, R. Welker, and E. Wimmer.** 2002. Interaction of the poliovirus receptor CD155 with the dynein light chain Tctex-1 and its implication for poliovirus pathogenesis. J. Biol. Chem. **277:**7897–7904.
32. **Nathanson, N., and A. D. Langmuir.** 1963. The Cutter incident: poliomyelitis following formaldehyde-inactivated poliovirus vaccination in the United States during the spring of 1955. III. Comparison of the clinical character of vaccinated and contact cases occurring after use of high rate lots of Cutter vaccine. Am. J. Hyg. **78:**61–81.
33. **Ohka, S., and A. Nomoto.** 2001. Recent insights into poliovirus pathogenesis. Trends. Microbiol. **9:**501–506.
34. **Ohka, S., H. Ohno, K. Tohyama, and A. Nomoto.** 2001. Basolateral sorting of human poliovirus receptor alpha involves an interaction with the mu1B subunit of the clathrin adaptor complex in polarized epithelial cells. Biochem. Biophys. Res. Commun. **287:**941–948.
35. **Ohka, S., W. X. Yang, E. Terada, K. Iwasaki, and A. Nomoto.** 1998. Retrograde transport of intact poliovirus through the axon via the fast transport system. Virology **250:**67–75.
36. **Ren, R., and V. R. Racaniello.** 1992. Poliovirus spreads from muscle to the central nervous system by neural pathways. J. Infect. Dis. **166:**747–752.
37. **Selinka, H. C., A. Zibert, and E. Wimmer.** 1991. Poliovirus can enter and infect mammalian cells by way of an intercellular adhesion molecule 1 pathway. Proc. Natl. Acad. Sci. USA **88:**3598–3602.
38. **Shiroki, K., T. Ishii, T. Aoki, M. Kobashi, S. Ohka, and A. Nomoto.** 1995. A new *cis*-acting element for RNA replication within the 5′ noncoding region of poliovirus type 1 RNA. J. Virol. **69:**6825–6832.
39. **Tokuyasu, K. T.** 1989. Use of poly(vinylpyrrolidone) and poly(vinyl alcohol) for cryoultramicrotomy. Histochem. J. **21:**163–171.
40. **Vallee, R. B., and M. P. Sheetz.** 1996. Targeting of motor proteins. Science **271:**1539–1544.
41. **Watanabe, T. K., T. Fujiwara, F. Shimizu, S. Okuno, M. Suzuki, E. Takahashi, Y. Nakamura, and Y. Hirai.** 1996. Cloning, expression, and mapping of TCTEL1, a putative human homologue of murine Tcte1, to 6q. Cytogenet. Cell Genet. **73:**153–156.
42. **White, D. M., K. Mansfield, and K. Kelleher.** 1996. Increased neurite outgrowth of cultured rat dorsal root ganglion cells following transection or inhibition of axonal transport of the sciatic nerve. Neurosci. Lett. **208:**93–96.
43. **Willingmann, P., H. Barnert, H. Zeichhardt, and K. O. Habermehl.** 1989. Recovery of structurally intact and infectious poliovirus type 1 from HeLa cells during receptor-mediated endocytosis. Virology **168:**417–420.
44. **Yang, W. X., T. Terasaki, K. Shiroki, S. Ohka, J. Aoki, S. Tanabe, T. Nomura, E. Terada, Y. Sugiyama, and A. Nomoto.** 1997. Efficient delivery of circulating poliovirus to the central nervous system independently of poliovirus receptor. Virology **229:**421–428.
45. **Zhuo, H., A. C. Lewin, E. T. Phillips, C. M. Sinclair, and C. J. Helke.** 1995. Inhibition of axoplasmic transport in the rat vagus nerve alters the numbers of neuropeptide and tyrosine hydroxylase messenger RNA-containing and immunoreactive visceral afferent neurons of the nodose ganglion. Neuroscience **66:**175–187.